# Optical Nanosensor Architecture for Cell-Signaling Molecules Using DNA Aptamer-Coated Carbon Nanotubes

**Tae-Gon Cha,[†] Benjamin A. Baker,[†] M. Dane Sauffer,[†] Janette Salgado,[†] David Jaroch,[‡] Jenna L. Rickus,[‡] D. Marshall Porterfield,[‡] and Jong Hyun Choi[†,*]**

[†]School of Mechanical Engineering, Bindley Bioscience Center, Birck Nanotechnology Center, Purdue University, West Lafayette, Indiana 47907, United States, and [‡]Weldon School of Biomedical Engineering, Agriculture and Biological Engineering, Physiological Sensing Facility, Bindley Bioscience Center, Purdue University, West Lafayette, Indiana 47907, United States

**ABSTRACT** We report a novel optical biosensor platform using near-infrared fluorescent single-walled carbon nanotubes (SWNTs) functionalized with target-recognizing aptamer DNA for noninvasively detecting cell-signaling molecules in real time. Photoluminescence (PL) emission of aptamer-coated SWNTs is modulated upon selectively binding to target molecules, which is exploited to detect insulin using an insulin-binding aptamer (IBA) as a molecular recognition element. We find that nanotube PL quenches upon insulin recognition *via* a photoinduced charge transfer mechanism with a quenching rate of $k_q = 5.85 \times 10^{14}\ M^{-1}\ s^{-1}$ and a diffusion–reaction rate of $k_r = 0.129\ s^{-1}$. Circular dichroism spectra reveal for the first time that IBA strands retain a four-stranded, parallel guanine quadruplex conformation on the nanotubes, ensuring target selectivity. We demonstrate that these IBA-functionalized SWNT sensors incorporated in a collagen extracellular matrix (ECM) can be regenerated by removing bound analytes through enzymatic proteolysis. As proof-of-concept, we show that the SWNT sensors embedded in the ECM promptly detect insulin secreted by cultured pancreatic INS-1 cells stimulated by glucose influx and report a gradient contour of insulin secretion profile. This novel design enables new types of label-free assays and noninvasive, *in situ*, real-time detection schemes for cell-signaling molecules.

**KEYWORDS:** aptamers · biosensors · carbon nanotubes · insulin · near-infrared fluorescence

Cell-signaling molecules and cytokines secreted from cells carry information about cell functions and transmit it between cells. They are thus crucial components in cell-to-cell communication and immune responses, and measurement of these messenger molecules *in situ* and in real time without perturbing the cells is important for understanding and regulating cell functions and immune systems. Current methodologies of detecting such messenger molecules include immunoassays such as radio immunoassay (RIA) and enzyme-linked immunosorbent assay (ELISA),[1−4] chromatographic methods,[5,6] and electrochemical measurements.[7−9] Immunoassays have been widely used for quick screening and quantitative measurements using antigen–antibody reaction due to the simplicity, relatively low cost, and availability of reliable commercial kits. The chromatographic methods offer reliable analyte selectivity since the separation steps are included. The electrochemical measurements typically demonstrate high detection sensitivity and short signal response time for electrical signal readouts. However, these assays typically require harvest of the analyte molecules from the cellular environments and transfer to a predetermined testbed of the sensors. Thus, current detection technologies are not capable of noninvasively transmitting comprehensive, dynamic information about molecular targets *in situ* and in real time directly from the secreting cells.

Single-walled carbon nanotubes (SWNTs) show promise to meet these requirements as optical sensing materials for cell-signaling molecules. Near-infrared (NIR) fluorescent properties render them excellent candidates for biological optical probes, since spectral information is transferred efficiently in the range of the so-called, tissue-transparent window, where absorption and autofluorescence by biological substances are minimal.[10−12] In contrast to commonly used organic fluorophores, carbon nanotubes are essentially nonphotobleaching and nonblinking, which are advantageous in long-term measurements.[13] SWNT photoluminescence (PL) is also very sensitive to molecular binding events at the sidewall, which may be exploited for optical detection schemes.[14−16] Additionally, the graphitic lattice allows noncovalent conjugation with biomolecular recognition elements such as DNA oligonucleotides, which preserves SWNT pristine electronic structures and thus their distinct optical signatures in aqueous solution.[17,18] Aptamers, single-stranded

* Address correspondence to jchoi@purdue.edu.

Received for review April 11, 2011 and accepted April 26, 2011.

**Published online April 26, 2011**
**10.1021/nn201323h**

nucleic acids or peptides, are of great interest for this purpose, since they recognize specific molecular targets with high binding affinity, just like antibodies that recognize antigens. Aptamer oligonucleotides are advantageous as molecular recognition probes owing to their excellent stability, nontoxicity, reproducible synthesis, and ease of manipulation.[19,20] Aptameric sequences are typically identified by evolutionary *in vitro* selection processes,[21,22] and several sequences have been shown to selectively bind cell-signaling molecules by forming a unique secondary structure called the guanine (G) quadruplex.[23,24]

In this work, we design and study novel optical nanosensor architecture based on NIR fluorescent SWNTs that noninvasively detect cell-signaling molecules in real time for the first time. Our new sensor platform includes SWNTs functionalized with aptamer DNA that modulate NIR emission upon recognizing signaling molecules secreted from live cells cultured on an extracellular matrix (ECM) in response to stimuli (Figure 1). We use insulin and insulin-binding aptamer (IBA) as a model system of the analyte and the molecular recognition element in this study. Insulin, a polypeptide hormone from mammalian pancreatic cells, was chosen because of its implications in diabetes, as it controls the glucose levels in blood, and insufficient release or loss of insulin results in the metabolic disease. A recently developed 30-base-long IBA sequence is used to selectively recognize insulin analytes.[25] We have discovered for the first time that this aptamer retains a four-stranded, parallel G quadruplex conformation on SWNTs, a necessity for specifically binding to the molecular targets. We find that highly selective PL quenching upon analyte binding is caused by a photoinduced charge transfer mechanism, and a one-dimensional diffusion−reaction model is developed to describe target recognition processes. It should be noted that our approach is completely different from the molecular beacon type of biosensing schemes where carbon nanotubes have been used as quenchers for organic fluorophores.[26,27] Finally, as proof-of-concept, we demonstrate that SWNT sensors embedded in a collagen ECM promptly detect insulin secreted by pancreatic INS-1 cells stimulated by glucose influx, demonstrating new types of label-free assays and *in situ*, real-time detection schemes for cell-signaling molecules.

## RESULTS AND DISCUSSION

**Design of Solution Phase Optical Biosensors.** We first functionalized carbon nanotubes noncovalently with 30-base-long, insulin-recognizing DNA (*i.e.*, insulin-binding aptamer) by two-stage dialysis against 1× Tris buffer. The dialysis processes replaced surfactants initially adsorbed on SWNTs with IBA strands *via* $\pi-\pi$ interaction and subsequently removed free oligonucleotides.[17]

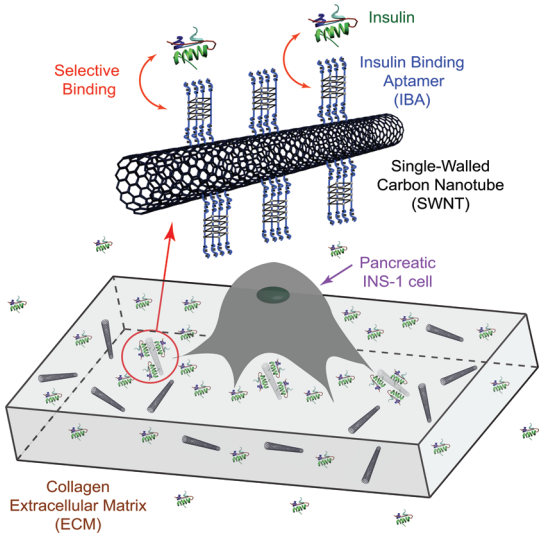


**Figure 1. Schematic of optical nanosensor architecture to measure insulin secreted from pancreatic INS-1 cells *in situ*, in real time. Near-IR fluorescent single-walled carbon nanotubes are noncovalently functionalized with insulin-binding aptamer DNA to recognize target insulin and optically report *via* a fluorescence quenching mechanism with high selectivity and sensitivity. The IBA-coated nanotubes embedded in a collagen extracellular matrix detect insulin secreted by cultured INS-1 cells stimulated by glucose influx.**

Figure 2a shows the photoluminescence excitation (PLE) spectra of IBA-functionalized SWNTs (~11.2 mg/L), showing distinct NIR emission signatures of several SWNT species. A chiral index (*n,m*) that identifies individual nanotube species is assigned to each peak.[28] Since CoMoCAT nanotubes that typically include a large population of small diameter ($d \approx 1$ nm) species are used in this study, strong fluorescence signals are observed from 950 to 1200 nm.[29] Addition of insulin to the IBA-SWNT solution at 470 $\mu$M introduced significant emission quenching in all the observed nanotubes (Figure 2b). This signal transduction is consistent, as there are no significant variations among different nanotube samples (Figure S1). The added insulin molecules diffuse in the solution and bind to IBAs on the nanotube sidewall, which results in SWNT signal transduction. The fluorescence spectra of SWNTs excited at 573 nm are shown as a function of insulin concentration in Figure 2c. The prominent (6,5) nanotubes emitting at ~995 nm and other species emission systematically quench with increasing insulin concentration from 0 to 470 $\mu$M. To determine the detection limit of IBA-functionalized SWNT sensors, the PL quenching of nanotubes is monitored at low insulin concentrations (Figure S2). The linear range of 0 to 180 nM insulin yields a detection limit of ~10 nM, which is higher than the insulin level in human blood, but sufficient to detect the insulin molecules in the human pancreas, as the average pancreatic insulin concentration is approximately 10 $\mu$M.[30−32] In contrast to the drastic PL quenching, the optical absorption of IBA-coated SWNTs remains relatively constant in the presence of analytes (Figure 2d).

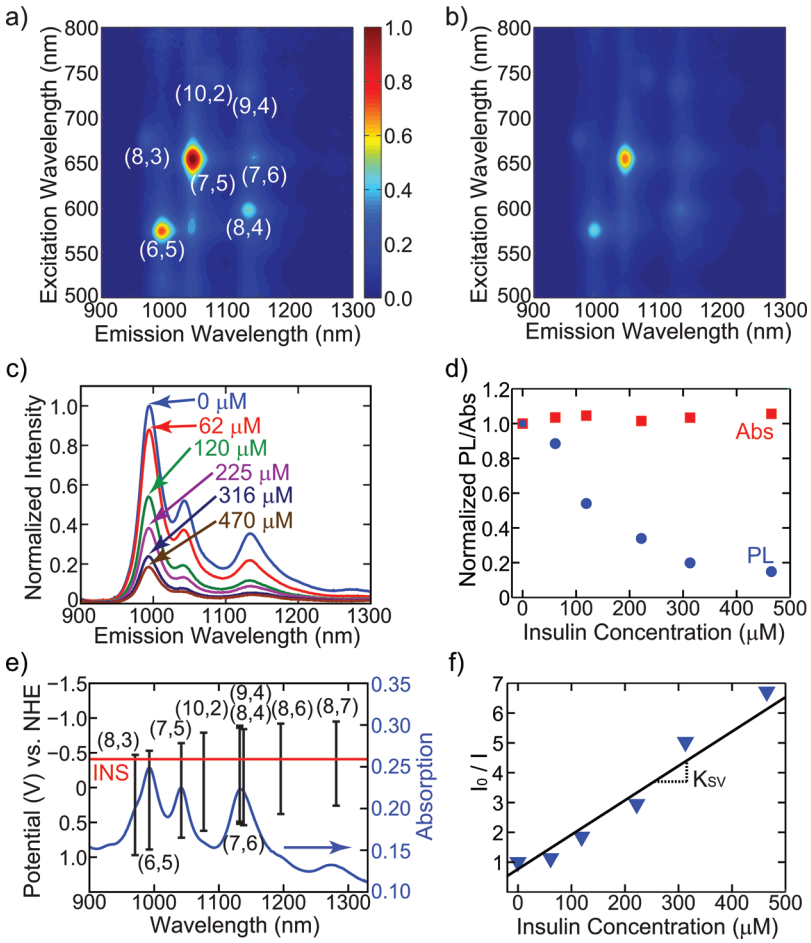


**Figure 2. NIR PL characteristics of IBA-coated SWNTs upon insulin recognition. (a) PLE spectra of IBA-SWNTs in 1× Tris buffer, showing distinct NIR emission signatures of several SWNT species. (b) PLE profile in the presence of insulin at 470 $\mu$M, demonstrating systematic PL decreases in all observed SWNT species. The color scale is the same as in (a). (c) SWNT-PL transduction as a function of insulin concentration from 0 to 470 $\mu$M. Nanotubes are excited at 573 nm. (d) Normalized intensities of PL (*blue*) and absorption (*red*) of the (6,5) SWNT peak as a function of insulin concentration. (e) Relative potential energies (*black*) of the valence and conduction bands of SWNT species[36,37] against normal hydrogen electrode are shown along with the optical absorption spectrum of IBA-SWNTs (*blue*). The reduction potential of insulin (*red*) is positioned between the two bands of SWNT species. The SWNT PL quenching upon insulin recognition is attributed to photoinduced electron transfer from the SWNT conduction band to the LUMO of the bound insulin. (f) Stern–Volmer plot of SWNT PL quenching. The slope, or Stern–Volmer constant, of the linear relationship is approximately $K_{SV} = 1.17 \times 10^4\ M^{-1}$.**

This observation suggests that the mechanism of PL transduction is photoinduced excited-state electron transfer from the SWNT conduction band to the lowest unoccupied molecular orbital (LUMO) of the bound analyte.[33,34] This principle is consistent given that the reduction potential of insulin (*red*) is approximately −0.409 V[35] and is positioned between the conduction and valence bands of SWNTs.[36,37] Figure 2e shows relative potential energies (*black*) of the valence and conduction bands of several nanotube species against normal hydrogen electrode (NHE) along with the optical absorption spectrum of IBA-SWNTs (*blue*).[36,37] The consistent quenching of all SWNT species observed in the PLE spectra also supports this mechanism (Figure 2a,b). The PL quenching kinetics can be determined from the Stern–Volmer formulation:

$$\frac{I_o}{I} = 1 + k_q \tau_o [Q] \qquad (1)$$

where $I$ and $I_o$ are PL intensities with and without quenching molecules, or Q. The slope of the linear relationship or Stern–Volmer constant is approximately $K_{SV} = k_q\tau_o = 1.17 \times 10^4\ M^{-1}$ (Figure 2f). The SWNT PL lifetime without a quencher ($\tau_o$) is assumed to be 20 ps,[38,39] and thus the PL quenching rate, $k_q$, is estimated to be roughly $5.85 \times 10^{14}\ M^{-1}\ s^{-1}$. These results strongly support photoinduced charge transfer as the predominant quenching mechanism.

Of considerable utility is that IBA-coated SWNTs do not optically respond to other interfering proteins (Figure 3a). To verify the target selectivity of the SWNT sensors, we examined control proteins with a wide range of isoelectric points (pI). Bovine serum albumin (BSA) and proteinase K have pI 4.8 and 8.9, which are correspondingly negatively and positively charged under our buffer conditions at pH 8.0. Both control proteins do not modulate the SWNT emission significantly, whereas 82% PL quenching

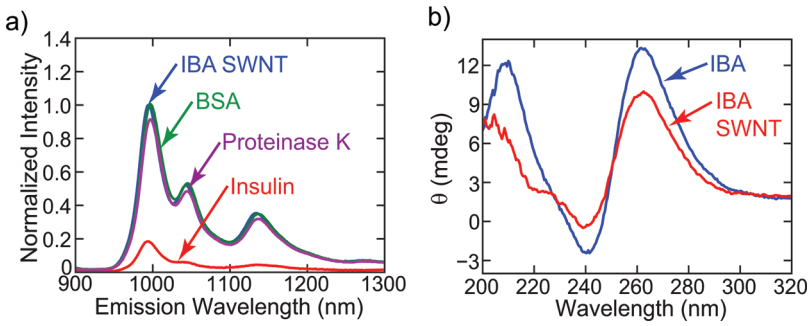


**Figure 3. Selectivity of IBA-coated SWNTs for insulin recognition. (a) SWNT PL intensities in the presence of control proteins with various isoelectric points (470 $\mu$M). The control proteins do not significantly modulate SWNT PL, whereas insulin immediately quenches nanotube emission. (b) Circular dichroism spectra of free IBA and IBA-SWNTs in buffer solution, suggesting a parallel, four-stranded G-quadruplex conformation of IBA both on and off the SWNT. This quadruplex structure is necessary for selectively binding to its target.**

is observed with insulin of the same concentration, demonstrating the analyte selectivity of IBA-SWNTs. This selectivity is highly dependent on the specific DNA aptamer sequence used as the molecular recognition element in the sensor platform. We note that the IBA forms a G-quadruplex conformation in order to selectively bind to target insulin.[25] We used circular dichroism (CD) spectroscopy to probe the secondary structure of the sequence, and the CD spectrum of IBA bound to SWNTs is compared to that of free strands in solution (Figure 3b). Both spectra show two positive peaks at approximately 263 and 209 nm and a negative valley at ~240 nm, which indicates a four-stranded, parallel G-quadruplex conformation.[40−42] Thus, these CD spectra suggest that the IBA strands retain the four-stranded, parallel G-quadruplex structure on and off the nanotubes. This observation is the first to monitor DNA G-quadruplex formation at the nanotube sidewall, rendering the SWNT sensors highly selective toward target insulin. The CD results imply that the optical biosensor architecture based on aptamer-coated SWNTs may be applicable to other sequences that require G-quadruplex formation for specific target recognition.

**Kinetic Model of Analyte Recognition Using SWNT PL Quenching.** To understand the kinetics of selective analyte binding that modulate SWNT emission, we develop a simple one-dimensional kinetic model based on molecular diffusion and reaction, while considering insulin diffusion and binding with IBA-SWNTs in solution.[43] We consider that the analyte molecules are transported by diffusion, while the fluorescent sensors are homogeneously distributed in the domain as shown in Figure 4a. The diffused analyte molecules are assumed to bind to the sensors irreversibly, resulting in PL signal transduction. The reaction between the analyte and sensor is expressed as

$$[\text{Analyte}] + [\text{Sensor}] \xrightarrow{k_r} [\text{Analyte}][\text{Sensor}] \quad (2)$$

where $k_r$ denotes the reaction rate. Initially, the analyte molecules ($U_o$) and sensor molecules ($V_o$) are uniformly situated in the space interval [0, $z$] and [0, $L$], respectively. Here, $U_o$ and $V_o$ denote the initial concentrations of analytes and sensors. The rate equation of the diffusion−reaction model is

$$\frac{\partial}{\partial t}u(x,t) = D\frac{\partial^2}{\partial x^2}u(x,t) - k_r u(x,t) \text{ for } x\in[0,L],\ t\geq 0 \quad (3)$$

Boundary conditions:

$$\frac{\partial}{\partial x}u(0,t) = \frac{\partial}{\partial x}u(L,t) = 0 \text{ for } t > 0 \quad (4)$$

Initial condition:

$$u(x,0) = \begin{cases} U_0 \text{ if } 0 < x < z \\ 0, \text{otherwise} \end{cases} \quad (5)$$

where $u(x, t)$ is the sensor concentration and $D$ is the diffusivity of analyte molecules in solution. Using separation of variables and Fourier series, an analytic solution is obtained:

$$u(x,t) = \frac{U_0 z}{L}e^{-k_r t} + \sum_{j=1}^{\infty}\frac{2U_0}{j\pi}\sin\left(\frac{j\pi}{L}z\right)e^{-\{D\left(\frac{j\pi}{L}\right)^2 + k_r\}t}\cos\left(\frac{j\pi}{L}\right)x \quad (6)$$

Considering the variation of the analyte concentration at a position $x$ at time $t$, the bound analytes and sensors in the time interval [0, $t$] are

$$\text{Bound } u(x,t) = \int_0^t k_r u(x,\tau)\,d\tau \quad (7)$$

$$\text{Bound } v(x,t) = \frac{1}{A} \quad (8)$$

where $A$ is the molar ratio between analyte molecules and sensors. We assume that the analytes do not fluoresce and that the PL intensity of the sensors decreases with a quenching constant, $\theta$, when the sensor recognizes the analyte. Then, the normalized PL signal can be expressed as

$$f(x,t) = 1 - \frac{(1-\theta)}{V_0 A}\int_0^t k_r u(x,\tau)\,d\tau \quad (9)$$

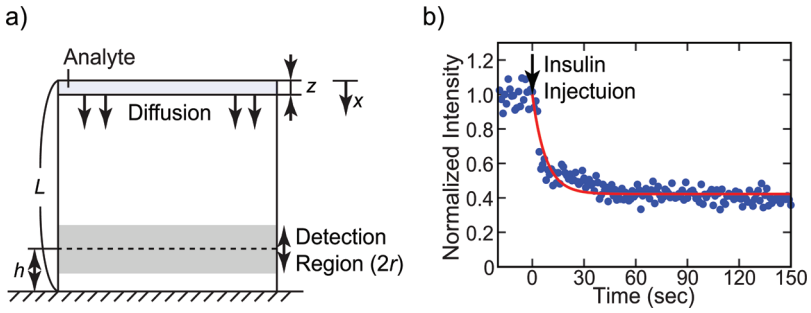


**Figure 4. Kinetics of SWNT PL signal changes upon recognition of the analyte molecules. (a) Domain for a one-dimensional kinetic diffusion−reaction model. In this model, the analyte molecules are initially located in $0 < x < z$ and diffuse into the domain at $t > 0$, while fluorescent sensors are uniformly distributed in the domain ($0 < x < L$). (b) PL quenching kinetics of IBA-SWNTs after 470 $\mu$M insulin addition. Experimental data points are shown in *blue*, while the theoretical model describes the kinetics in *red*.**

We consider the detection region of $[x-r, x+r]$, and the final emission signal becomes

$$F(t) = \int_{x-r}^{x+r} f(x, t)\, dt \qquad (10)$$

We used this simple one-dimensional diffusion−reaction model to determine the reaction rate between insulin and IBA-SWNTs in solution. To experimentally determine the kinetics of insulin recognition by IBA-SWNTs, we measured nanotube emission over 150 s after insulin injection (Figure 4b). In our experiments, $z$ and $L$ were approximately 377 $\mu$m and 1.39 mm, while the focal length of the objective lens was $h = 190$ $\mu$m and the detection region or the field of depth was approximately $2r = 0.4$ $\mu$m. The diffusivity of insulin is estimated at $D = 150$ $\mu m^2/s$.[44] As shown in Figure 4b, the kinetic model describes the experimental data well and suggests a diffusion−reaction rate of $k_r = 0.129$ $s^{-1}$, which is similar to that of SWNT reaction with biomolecules reported by Satishkumar *et al.*[33]

**Integration of SWNT Sensors into an ECM.** To interface nanotubes with cellular environments, we first incorporated IBA-coated SWNTs into a biocompatible collagen ECM that can be used as a cell culture platform since it facilitates the growth and differentiation of attached cells.[45,46] The collagen ECM immobilizes IBA-SWNTs inside its porous structure and prevents them from directly contacting cultured living cells. The immobilized nanotubes appear to be randomly spread in the matrix, as shown in the NIR PL images (Figure 5a,b), where a 658 nm laser was used for excitation and SWNT emission longer than 850 nm was collected under an inverted microscope. This excitation energy produces the most prominent (7,5) nanotube emission at ~1044 nm among several SWNT species (Figures S3 and 5c).[29] The emission characteristics of SWNTs immobilized in the ECM remain almost constant; the PL wavelength of each species corresponds to that of nanotubes uniformly dispersed in solution (Figure S3). After addition of insulin at 470 $\mu$M, a drastic SWNT PL quenching is observed in both the NIR images (Figure 5b) and the corresponding spectra (Figure S4), similar to what is seen in solution phase. The porosity of the collagen ECM structure allows small molecules such as insulin (5.8 kDa) to diffuse into the matrix and react with immobilized IBA-SWNTs, resulting in emission transduction.[47]

The quenched SWNT fluorescence is restored by incorporating α-chymotrypsin, an enzyme that digests insulin molecules.[9,48] After added to the solution at 49 $\mu$M, α-chymotrypsin (25 kDa) diffuses into the ECM and hydrolyzes the insulin bound to the nanotube surface, resulting in full recovery of SWNT-PL (from *red* to *green* in Figure 5c). This proteolysis process typically takes approximately 1 h. The IBA-SWNTs in the ECM are reusable after washing with excess buffer to remove the enzyme and insulin fragments. Thus, subsequent addition of insulin to the regenerated nanotube sensors reinduces the PL modulation, which can then be recovered with α-chymotrypsin. Figure 5d shows two cycles of insulin binding and removal by proteolysis. The recycled SWNT sensors were examined two months later, and their optical signals were persistent, which may be readily used for target recognition again. In theory, these sensors may be regenerated for an indefinite number of cycles. Given the SWNTs' photostable optical properties without photobleaching, the IBA-SNWT sensors are capable of a large number of uses and long-term operation and have a potential for reusable sensors in the cellular environment.

**Insulin Detection Secreted from Pancreatic INS-1.** As proof-of-concept, we demonstrated *in situ*, noninvasive, real-time detection of insulin secreted from pancreatic INS-1 cells. Approximately $7.5 \times 10^5$ cells were plated and cultured on a collagen ECM that contained the immobilized IBA-SWNTs. After incubation for 24 h at 37 °C, the cells were visualized using differential interference contrast (DIC) microscopy (Figure 6a), while NIR PL images of SWNTs were recorded every second for 5 min after each glucose injection. During this period, high doses of glucose were added three times to facilitate insulin secretion from the cells.[49,50] Figure 6b,c shows the NIR PL images before and 15 min after glucose addition. The PL quenching map overlaid with the DIC cell image (Figure 6d) is constructed by subtracting the PL intensity

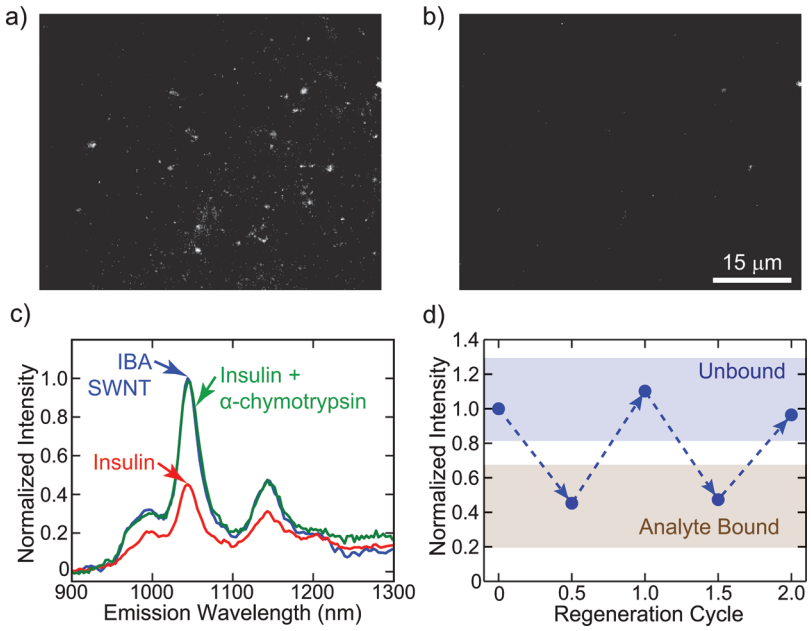


**Figure 5. Reversible fluorescence of IBA-SWNTs immobilized in a collagen ECM. NIR PL images of IBA-SWNTs embedded in an ECM (a) before and (b) after insulin injection at 470 $\mu$M. (c) The corresponding spectra of NIR images (a) and (b) are shown in *blue* and *red*, respectively. The quenched SWNT fluorescence is recovered from *red* to *green* after digesting the bound insulin using 49 $\mu$M $\alpha$-chymotrypsin. The PL recovery after $\alpha$-chymotrypsin addition indicates regeneration of IBA-SWNT sensors *via* proteolysis of insulin. (d) Two PL regeneration cycles based on (7,5) nanotube PL intensities with alternating injection of insulin and $\alpha$-chymotrypsin. The nanotubes are excited by a 658 nm diode laser.**

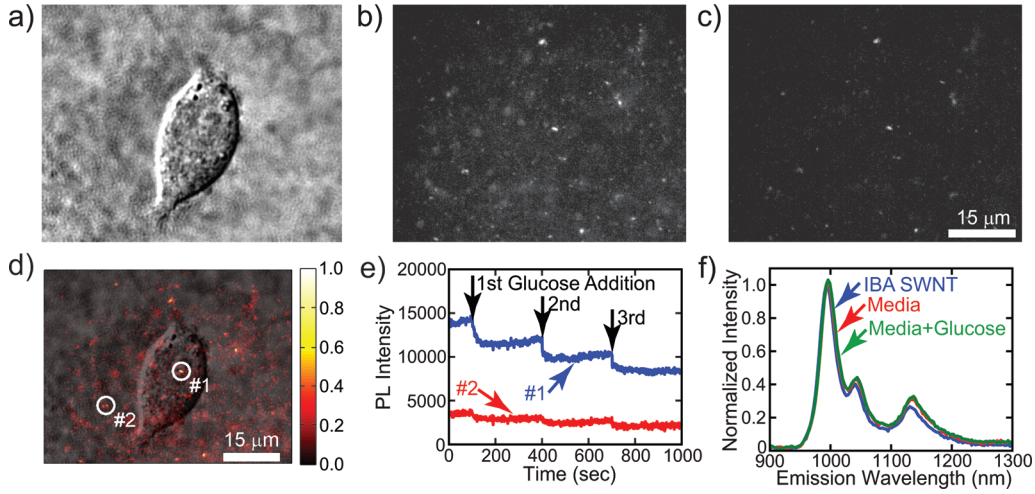


**Figure 6. *In situ*, real-time detection of insulin secreted from cultured pancreatic INS-1 cells on a collagen ECM containing NIR fluorescent IBA-SWNTs. (a) Differential interference contrast image of a single INS-1 cell. NIR PL images of IBA-SWNTs in the ECM before (b) and 15 min after (c) adding glucose in order to facilitate the insulin secretion from the cells. (d) SWNT PL quenching map (*i.e.*, spatially resolved insulin secretion profile) overlaid with the DIC cell image in (a). The pseudocolored map is constructed by subtracting the intensity of each pixel in (c) from that in (b). The scale bar indicates relative quenching level. (e) PL intensities at two locations in (d) as a function of time. (f) The PL intensity of IBA-SWNTs (*blue*) remains constant in the presence of cell culture media, RPMI 1640 (*red*), or glucose in media at 0.3 M (*green*). The persistent SWNT emission confirms that IBA-SWNTs recognize target insulin and do not optically respond to other molecules.**

of each pixel in Figure 6c from that in Figure 6b, so *white* indicates maximum PL transduction of IBA-SWNTs under our experimental conditions. This pseudocolored map represents the spatially resolved insulin secretion profile around the observed cell; a higher degree of nanotube quenching is observed near the cell, and the quenching level decreases away from the cell. The added glucose facilitates cellular secretion of insulin molecules that are transported away from the cell by diffusion, which is shown in the plotted gradient contour of insulin outflux. The PL intensity at two positions in Figure 6d is plotted as a function of time in Figure 6e. The time-resolved insulin profiles at these locations show that each glucose addition event promotes metabolic activities in the cells, which in turn results in secretion and diffusion of insulin molecules. The SWNT sensors at location #1, which

is beneath the observed cell, demonstrate greater signal transduction compared to those at location #2, away from the cell, indicating outflux of insulin molecules. We confirm that this PL transduction is not caused by any molecules other than analyte insulin. As shown in Figure 6f, cell culture media (RPMI 1640) or high doses of glucose (0.3 M) do not result in any apparent changes in nanotube emission signals.

## CONCLUSION

In summary, we have shown that DNA aptamer-coated SWNTs can form the basis for label-free optical nanosensors to remotely monitor cell-signaling molecules in real time. The carbon nanotubes integrated with an insulin-recognizing DNA sequence demonstrate strong PL transductions upon insulin binding *via* a photoinduced charge transfer mechanism. Quantitative measurements of SWNT PL quenching suggest a detection limit of ~10 nM for insulin. The CD measurement reveals that a four-stranded, parallel G-quadruplex structure of the aptamer DNA is retained on the SWNT, allowing the high target selectivity. The Stern–Volmer plot yields a PL quenching rate of approximately $k_q = 5.85 \times 10^{14}\ M^{-1}\ s^{-1}$, while a one-dimensional kinetic model for analyte recognition suggests a diffusion–reaction rate of $k_r = 0.129\ s^{-1}$. We have demonstrated that the SWNT sensors embedded in a biocompatible collagen ECM can be regenerated by enzymatic proteolysis using α-chymotrypsin. The optical sensors are capable of reporting a gradient contour of insulin outflux from cultured pancreatic INS-1 cells stimulated by glucose, demonstrating new types of *in situ*, real-time detection schemes for cell-signaling molecules. The biosensor architecture developed in this study may be applied to other analytes of interest by incorporating appropriate aptamer sequences and could improve the detection sensitivity to the single analyte molecule level if individual nanotubes are examined.[51–53]

## METHODS

**Materials.** Insulin-binding aptamer (IBA: 5′-GGT GGT GGG GGG GGT TGG TAG GGT GTC TTC-3′) strands were custom-synthesized and purchased from Integrated DNA Technologies, Inc. Several DNA sequences have been reported to selectively bind to insulin molecules. For example, the insulin-linked polymorphic region sequence ($ILPR_2$: 5′-ACA GGG GTG TGG GGA CAG GGG TGT GGG G-3′) can capture insulin molecules.[24] Because the IBA sequence reportedly has a higher binding affinity to insulin than $ILPR_2$,[25] the IBA sequence was selected as molecular recognition elements for DNA-coated SWNT sensors in this study.

CoMoCAT SWNTs were purchased from Southwest Nanotechnology, while sodium cholate was obtained from Affymetrix Inc. Insulin from bovine pancreas, BSA, proteinase K, β-mercaptoethanol, HEPES buffer, Na-pyruvate, L-glutamine, penicillin, and streptomycin were purchased from Sigma Aldrich. We obtained fetal calf serum, trypsin EDTA solution, RPMI 1640 medium, and phosphate-buffered saline (PBS) from Invitrogen, while rat tail collagen I was purchased from BD Bioscience.

**SWNT Suspension.** Aqueous suspensions of sodium cholate (SC)-coated SWNTs (~181.10 mg/L) were prepared by tip sonication at 20 W for 1 h, followed by ultracentrifugation at 30 000 rpm.[29] After centrifugation, the supernatant was carefully decanted to obtain homogeneous surfactant-suspended SWNT samples, which were separated from the denser catalyst particles, bundles, and impurities. In order to noncovalently functionalize nanotubes with DNA, approximately 91 μM IBAs was added to the SC-SWNT solution, which was dialyzed using a 12–14 kDa porous membrane (Fisherbrand) against 1× Tris buffer for 24 h.[16] The buffer was changed every 4 h during the dialysis, and aqueous SWNT solutions were maintained at pH 8.0 using NaOH solution. To remove free DNA from the SWNT suspension, a second dialysis using a 100 kDa membrane (Fisherbrand) was performed for 24 h.

**Integration of IBA-SWNTs in the ECM.** Collagen ECM was prepared following the procedure described by Han *et al.*[47] Approximately, 93 μL of a 0.1 M NaOH solution was added to 410 μL of rat tail collagen I (3–4 mg/mL) to achieve pH 7.5. Then, 20 mL of 1× PBS buffer and 5 mL of IBA-coated SWNTs were added to a pH-controlled collagen solution and stirred for 5 min in an ice bath to maintain collagen stability. A 100 μL aliquot of collagen solution containing IBA-SWNTs was then pipetted onto a glass bottom Petri dish (MatTek Corp.) and polymerized for 1 h at 40 °C. During polymerization, parafilm was wrapped over the Petri dish to prevent the solution from evaporating.

**Cellular Insulin Detection.** Pancreatic INS-1 cells were cultured in RPMI 1640 medium supplemented with 10% fetal calf serum, 50 μM β-mercaptoethanol, 10 mM HEPES, 1 mM Na-pyruvate, 2 mM L-glutamine, 100 U/mL penicillin, and 100 μg of streptomycin on 10 cm BD Falcon polystyrene tissue culture dishes at 37 °C and a 5% $CO_2$ atmosphere. Once the cells reached 90% confluency, they were detached from the culture dish using a 0.05% trypsin EDTA solution. The cells were then centrifuged and resuspended in 4 mL of growth medium. Prior to plating, the IBA-SWNT-containing collagen ECM was sterilized with UV light for 20 min. Suspended cells (~750 cells/μL) were then pipetted onto three spots (~0.3 mL per spot) on the sterilized collagen ECM and incubated for 24 h in 3 mL of RPMI 1640 medium.

**Optical Measurements.** NIR fluorescence spectra of IBA-coated SWNTs in solution were measured using a Horiba Jobin Yvon Fluorolog-3 spectrofluorometer with a liquid $N_2$-cooled InGaAs detector. The integration time for measuring a single point was 10 s, and the slit widths of excitation and emission are 5 and 10 nm, respectively. A home-built microscope system measured NIR fluorescence images and spectra of IBA-SWNTs in the collagen ECM using an OMA-V 2-D liquid $N_2$-cooled InGaAs camera (320 × 256 pixels, Princeton Instruments) with a 658 nm diode laser excitation. A Zeiss Plan-Apochromat 63×/1.4 oil-immersion objective lens was used to collect the nanotube emission. Optical absorption spectra were measured with a Perkin-Elmer Lambda 950 UV/vis/NIR spectrophotometer. CD spectra of free IBA strands and IBA-SWNTs in solution were measured with a JASCO J-810 spectropolarimeter using a 0.1 cm path length quartz cuvette at room temperature.

*Acknowledgment.* This work was supported by National Science Foundation and Purdue University. J.H.C. acknowledges a NSF CAREER Award, and B.A.B. is grateful for a NSF Graduate Research Fellowship. D.M.P acknowledges a NSF Instrumentation for Biological Research grant. This project was also supported by the Indiana Clinical and Translational Science Institute funded in part by Grant Number (RR025761) from the National Institutes of Health, National Center for Research Resources, Clinical and Translational Sciences Award. The INS-1 cells were provided as a kind gift by Dr. Raghu Mirmira of Indiana University.

*Supporting Information Available:* The determination of the detection limit of IBA-SWNT sensors; spectra of IBA-SWNTs in buffer solution and in an ECM; regeneration of SWNT sensors in solution; polarization of IBA-SWNTs in the collagen ECM. This material is available free of charge *via* the Internet at http://pubs.acs.org.

## REFERENCES AND NOTES


1. Arimura, A.; Somogyvarivigh, A.; Miyata, A.; Mizuno, K.; Coy, D. H.; Kitada, C. Tissue Distribution of Pacap as Determined by Ria - Highly Abundant in the Rat-Brain and Testes. *Endocrinology* **1991**, *129*, 2787–2789.
2. Clark, M. F.; Lister, R. M.; Barjoseph, M. Elisa Techniques. *Method Enzymol.* **1986**, *118*, 742–766.
3. Gosling, J. P. A Decade of Development in Immunoassay Methodology. *Clin. Chem.* **1990**, *36*, 1408–1427.
4. Wisdom, G. B. Enzyme-Immunoassay. *Clin. Chem.* **1976**, *22*, 1243–1255.
5. Pingoud, V.; Trautschold, I. High-Performance Liquid-Chromatography of Iodine-Labeled Insulin and Glucagon Derivatives with Online Gamma-Detection. *Anal. Biochem.* **1984**, *140*, 305–314.
6. Sarmento, B.; Ribeiro, A.; Veiga, F.; Ferreira, D. Development and Validation of a Rapid Reversed-Phase HPLC Method for the Determination of Insulin from Nanoparticulate Systems. *Biomed. Chromatogr.* **2006**, *20*, 898–903.
7. Drummond, T. G.; Hill, M. G.; Barton, J. K. Electrochemical DNA Sensors. *Nat. Biotechnol.* **2003**, *21*, 1192–1199.
8. Salimi, A.; Noorbakhash, A.; Sharifi, E.; Semnani, A. Highly Sensitive Sensor for Picomolar Detection of Insulin at Physiological pH, Using GC Electrode Modified with Guanine and Electrodeposited Nickel Oxide Nanoparticles. *Biosens. Bioelectron.* **2008**, *24*, 792–798.
9. Wang, Y.; Li, J. H. A Carbon Nanotubes Assisted Strategy for Insulin Detection and Insulin Proteolysis Assay. *Anal. Chim. Acta* **2009**, *650*, 49–53.
10. Choi, J. H.; Nguyen, F. T.; Barone, P. W.; Heller, D. A.; Moll, A. E.; Patel, D.; Boppart, S. A.; Strano, M. S. Multimodal Biomedical Imaging with Asymmetric Single-Walled Carbon Nanotube/Iron Oxide Nanoparticle Complexes. *Nano Lett.* **2007**, *7*, 861–867.
11. Kim, S.; Lim, Y. T.; Soltesz, E. G.; De Grand, A. M.; Lee, J.; Nakayama, A.; Parker, J. A.; Mihaljevic, T.; Laurence, R. G.; Dor, D. M.; *et al*. Near-Infrared Fluorescent Type II Quantum Dots for Sentinel Lymph Node Mapping. *Nat. Biotechnol.* **2004**, *22*, 93–97.
12. Weissleder, R.; Ntziachristos, V. Shedding Light onto Live Molecular Targets. *Nat. Med.* **2003**, *9*, 123–128.
13. Carlson, L. J.; Krauss, T. D. Photophysics of Individual Single-Walled Carbon Nanotubes. *Acc. Chem. Res.* **2008**, *41*, 235–243.
14. Cherukuri, P.; Gannon, C. J.; Leeuw, T. K.; Schmidt, H. K.; Smalley, R. E.; Curley, S. A.; Weisman, R. B. Mammalian Pharmacokinetics of Carbon Nanotubes Using Intrinsic Near-Infrared Fluorescence. *Proc. Natl. Acad. Sci. U. S. A.* **2006**, *103*, 18882–18886.
15. Choi, J. H.; Strano, M. S. Solvatochromism in Single-Walled Carbon Nanotubes. *Appl. Phys. Lett.* **2007**, *90*, 223114.
16. Jeng, E. S.; Moll, A. E.; Roy, A. C.; Gastala, J. B.; Strano, M. S. Detection of DNA Hybridization Using the Near-Infrared Band-Gap Fluorescence of Single-Walled Carbon Nanotubes. *Nano Lett.* **2006**, *6*, 371–375.
17. Barone, P. W.; Baik, S.; Heller, D. A.; Strano, M. S. Near-Infrared Optical Sensors Based on Single-Walled Carbon Nanotubes. *Nat. Mater.* **2005**, *4*, 86–92.
18. Chen, J.; Liu, H. Y.; Weimer, W. A.; Halls, M. D.; Waldeck, D. H.; Walker, G. C. Noncovalent Engineering of Carbon Nanotube Surfaces by Rigid, Functional Conjugated Polymers. *J. Am. Chem. Soc.* **2002**, *124*, 9034–9035.
19. Lee, J. F.; Stovall, G. M.; Ellington, A. D. Aptamer Therapeutics Advance. *Curr. Opin. Chem. Biol.* **2006**, *10*, 282–289.
20. Willner, I.; Zayats, M. Electronic Aptamer-Based Sensors. *Angew. Chem., Int. Ed.* **2007**, *46*, 6408–6418.
21. Daniels, D. A.; Chen, H.; Hicke, B. J.; Swiderek, K. M.; Gold, L. A Tenascin-C Aptamer Identified by Tumor Cell SELEX: Systematic Evolution of Ligands by Exponential Enrichment. *Proc. Natl. Acad. Sci. U. S. A.* **2003**, *100*, 15416–15421.
22. Klug, S. J.; Famulok, M. All You Wanted to Know About SELEX. *Mol. Biol. Rep.* **1994**, *20*, 97–107.
23. Choi, J. H.; Chen, K. H.; Strano, M. S. Aptamer-Capped Nanocrystal Quantum Dots: a New Method for Label-Free Protein Detection. *J. Am. Chem. Soc.* **2006**, *128*, 15584–15585.
24. Connor, A. C.; Frederick, K. A.; Morgan, E. J.; McGown, L. B. Insulin Capture by an Insulin-Linked Polymorphic Region G-Quadruplex DNA Oligonucleotide. *J. Am. Chem. Soc.* **2006**, *128*, 4986–4991.
25. Yoshida, W.; Mochizuki, E.; Takase, M.; Hasegawa, H.; Morita, Y.; Yamazaki, H.; Sode, K.; Ikebukuro, K. Selection of DNA Aptamers against Insulin and Construction of an Aptameric Enzyme Subunit for Insulin Sensing. *Biosens. Bioelectron.* **2009**, *24*, 1116–1120.
26. Zhu, Z.; Yang, R. H.; You, M. X.; Zhang, X. L.; Wu, Y. R.; Tan, W. H. Single-Walled Carbon Nanotube as an Effective Quencher. *Anal. Bioanal. Chem. 396*, 73−83.
27. Yang, R. H.; Jin, J. Y.; Chen, Y.; Shao, N.; Kang, H. Z.; Xiao, Z.; Tang, Z. W.; Wu, Y. R.; Zhu, Z.; Tan, W. H. Carbon Nanotube-Quenched Fluorescent Oligonucleotides: Probes that Fluoresce upon Hybridization. *J. Am. Chem. Soc.* **2008**, *130*, 8351–8358.
28. Bachilo, S. M.; Strano, M. S.; Kittrell, C.; Hauge, R. H.; Smalley, R. E.; Weisman, R. B. Structure-Assigned Optical Spectra of Single-Walled Carbon Nanotubes. *Science* **2002**, *298*, 2361–2366.
29. Bachilo, S. M.; Balzano, L.; Herrera, J. E.; Pompeo, F.; Resasco, D. E.; Weisman, R. B. Narrow (n,m)-Distribution of Single-Walled Carbon Nanotubes Grown Using a Solid Supported Catalyst. *J. Am. Chem. Soc.* **2003**, *125*, 11186–11187.
30. Saisho, Y.; Butler, A. E.; Meier, J. J.; Monchamp, T.; Allen-Auerbach, M.; Rizza, R. A.; Butler, P. C. Pancreas Volumes in Humans from Birth to Age One Hundred Taking into Account Sex, Obesity, and Presence of Type-2 Diabetes. *Clin. Anat.* **2007**, *20*, 933–942.
31. Scott, D. A.; Fisher, A. M. The Insulin and the Zinc Content of Normal and Diabetic Pancreas. *J. Clin. Invest.* **1938**, *17*, 725–728.
32. Volund, A.; Brange, J.; Drejer, K.; Jensen, I.; Markussen, J.; Ribel, U.; Sorensen, A. R.; Schlichtkrull, J. In vitro and In vivo Potency of Insulin Analogs Designed for Clinical Use. *Diabetic Med.* **1991**, *8*, 839–847.
33. Satishkumar, B. C.; Brown, L. O.; Gao, Y.; Wang, C. C.; Wang, H. L.; Doorn, S. K. Reversible Fluorescence Quenching in Carbon Nanotubes for Biomolecular Sensing. *Nat. Nanotechnol.* **2007**, *2*, 560–564.
34. Wang, J.; Wang, D. L.; Moses, D.; Heeger, A. J. Dynamic Quenching of 5-(2′-Ethyl-Hexyloxy)-*p*-Phenylene Vinylene (MEH-PPV) by Charge Transfer to a C-60 Derivative in Solution. *J. Appl. Polym. Sci.* **2001**, *82*, 2553–2557.
35. Cecil, R.; Weitzman, P. D. Electroreduction of Disulphide Bonds of Insulin and Other Proteins. *Biochem. J.* **1964**, *93*, 1–11.
36. O'Connell, M. J.; Eibergen, E. E.; Doorn, S. K. Chiral Selectivity in the Charge-Transfer Bleaching of Single-Walled Carbon-Nanotube Spectra. *Nat. Mater.* **2005**, *4*, 412–418.
37. Tanaka, Y.; Hirana, Y.; Niidome, Y.; Kato, K.; Saito, S.; Nakashima, N. Experimentally Determined Redox Potentials of Individual (n,m) Single-Walled Carbon Nanotubes. *Angew. Chem., Int. Ed.* **2009**, *48*, 7655–7659.
38. Matsuda, K.; Miyauchi, Y.; Sakashita, T.; Kanemitsu, Y. Nonradiative Exciton Decay Dynamics in Hole-Doped Single-Walled Carbon Nanotubes. *Phys. Rev. B* **2010**, *81*, 033409.
39. Wang, F.; Dukovic, G.; Brus, L. E.; Heinz, T. F. Time-Resolved Fluorescence of Carbon Nanotubes and Its Implication for Radiative Lifetimes. *Phys. Rev. Lett.* **2004**, *92*, 177401.

40. Giraldo, R.; Suzuki, M.; Chapman, L.; Rhodes, D. Promotion of Parallel DNA Quadruplexes by a Yeast Telomere Binding-Protein - a Circular-Dichroism Study. *Proc. Natl. Acad. Sci. U. S. A.* **1994**, *91*, 7658–7662.
41. Gray, D. M.; Ratliff, R. L.; Vaughan, M. R. Circular-Dichroism Spectroscopy of DNA. *Method Enzymol.* **1992**, *211*, 389–406.
42. Paramasivan, S.; Rujan, I.; Bolton, P. H. Circular Dichroism of Quadruplex DNAs: Applications to Structure, Cation Effects and Ligand Binding. *Methods* **2007**, *43*, 324–331.
43. Hinow, P.; Rogers, C. E.; Barbieri, C. E.; Pietenpol, J. A.; Kenworthy, A. K.; DiBenedetto, E. The DNA Binding Activity of P53 Displays Reaction-Diffusion Kinetics. *Biophys. J.* **2006**, *91*, 330–342.
44. Vogel, S. In *Life's Devices: The Physical World of Animals and Plants*; Princeton University Press: Princeton, 1988; p 164.
45. Kleinman, H. K.; Klebe, R. J.; Martin, G. R. Role of Collagenous Matrices in the Adhesion and Growth of Cells. *J. Cell Biol.* **1981**, *88*, 473–485.
46. Merzak, A.; Koochekpour, S.; Pilkington, G. J. Adhesion of Human Glioma Cell-Lines to Fibronectin, Laminin, Vitronectin and Collagen I is Modulated by Gangliosides In-Vitro. *Cell Adhes. Commun.* **1995**, *3*, 27–43.
47. Han, B.; Miller, J. D.; Jung, J. K. Freezing-Induced Fluid-Matrix Interaction in Poroelastic Material. *J. Biomech. Eng.-Trans. ASME* **2009**, *131*, 021002.
48. Schilling, R. J.; Mitra, A. K. Degradation of Insulin by Trypsin and Alpha-Chymotrypsin. *Pharm. Res.* **1991**, *8*, 721–727.
49. Asfari, M.; Janjic, D.; Meda, P.; Li, G. D.; Halban, P. A.; Wollheim, C. B. Establishment of 2-Mercaptoethanol-Dependent Differentiated Insulin-Secreting Cell-Lines. *Endocrinology* **1992**, *130*, 167–178.
50. Hohmeier, H. E.; Mulder, H.; Chen, G. X.; Henkel-Rieger, R.; Prentki, M.; Newgard, C. B. Isolation of INS-1-Derived Cell Lines with Robust ATP-Sensitive K+ Channel-Dependent and Independent Glucose-Stimulated Insulin Secretion. *Diabetes* **2000**, *49*, 424–430.
51. Hartschuh, A.; Qian, H.; Georgi, C.; Boehmler, M.; Novotny, L. Tip-Enhanced Near-Field Optical Microscopy of Carbon Nanotubes. *Anal. Bioanal. Chem.* **2009**, *394*, 1787–1795.
52. Lefebvre, J.; Finnie, P. Excited Excitonic States in Single-Walled Carbon Nanotubes. *Nano Lett.* **2008**, *8*, 1890–1895.
53. Tsyboulski, D. A.; Bachilo, S. M.; Weisman, R. B. Versatile Visualization of Individual Single-Walled Carbon Nanotubes with Near-Infrared Fluorescence Microscopy. *Nano Lett.* **2005**, *5*, 975–979.